The Astrophysical Journal, 651:1238–1244, 2006 November 10

TWO SUCCESSIVE CORONAL MASS EJECTIONS DRIVEN BY THE KINK AND DRAINAGE INSTABILITIES OF AN ERUPTIVE PROMINENCE

G. P. Zhou, J. X. Wang, and J. Zhang
National Astronomical Observatories, Chinese Academy of Sciences, Beijing 100012, China; zhougp@ourstar.bao.ac.cn

P. F. Chen
Department of Astronomy, Nanjing University, Nanjing 210093, China

H. S. Ji
Purple Mountain Observatory, 2 Beijing Xi Lu, Nanjing 210008, China

and

K. Dere
George Mason University, 4400 University Drive, Fairfax, VA 22030
Received 2006 January 11; accepted 2006 July 17

ABSTRACT

We describe a clear case of the initiation of a propagating bright arc and a CME on 2002 December 28, which were associated with an eruptive prominence. In EIT 304 and 195 Å images, a very long filament showed evidence of severe twisting in one of its fragments, which appeared as a prominence on December 26; then, the prominence showed the conversion of its twist into writhe. Two days later, the prominence displayed a slow rising motion for hours. Internal twisting and mass motion took place before the rapid acceleration and final eruption. The propagating bright arc and the following CME corresponded to the early rising and the subsequently eruptive phases of the prominence, respectively. Signatures of magnetic reconnection, i.e., a cusp structure and postflare loops in EUV wave bands and hard X-ray sources in the corona, were observed after the prominence eruption. It appears that the kink instability and the mass drainage in the prominence played key roles in triggering the initiation of the CME. However, the rather impulsive acceleration of the CME resulted from magnetic reconnection beneath the filament.

Subject headings: Sun: coronal mass ejections (CMEs) — Sun: prominences

Online material: color figures, mpeg animation

1. INTRODUCTION

Coronal mass ejections (CMEs) are the most important manifestation of solar activity that drives the space weather near Earth (Gosling 1993). A lot of CMEs are observed by coronagraphs above the occulted solar limb. However, the corresponding source regions near the solar surface are obscure and the processes of CME initiation from lower corona are lacking direct observations. Therefore, the physics of CME initiation remains a mystery in solar astrophysics.

Several mechanisms have been proposed to trigger the CME initiation, e.g., the photospheric converging and shear motions (Forbes et al. 1994; Mikic & Linker 1994; Antiochos et al. 1994), flux emergence (Feynman & Martin 1995; Chen & Shibata 2000), and cancellation (Zhang et al. 2001). Recently, kink instability of coronal flux ropes has attracted more and more attention. Sakurai (1976) was the first to attribute kinked flux ropes to eruptive filaments. Plunkett et al. (2000) found that the writhing took place in a prominence-associated CME. Lately, filament eruptions resulting from the kink instability were reported by several authors (Rust 2003; Rust & LaBonte 2005; Williams et al. 2005). In these studies, filaments were taken as magnetic flux ropes, which appeared to be a central component in theoretical modelings. Another line of thought in triggering the instability is flux rope catastrophe (e.g., Hu 2005). In addition, the drainage of plasma from a prominence is also a possible cause for the flux rope to be accelerated (Tandberg-Hanssen 1974; Gilbert et al. 2000). Moreover, there have been many analytical and numerical models (e.g., Bety 2001; Lin & Forbes 2000; Gerrard et al. 2001; Fan & Gibson 2004; Török & Kliem 2005), in which magnetic reconnection is found to play an important role in accelerating the flux rope/prominence after the kink instability or catastrophe occurs. On the other hand, the magnetic breakout model (Antiochos et al. 1999) suggests that the magnetic reconnection at the top of sheared core fields is fundamental in triggering CME onsets. Very recently, a two-current-sheet reconnection scenario has been proposed to account for both the magnetic breakout and the standard flare models (Zhang et al. 2006).

As there is a close correlation between filament eruption and CMEs (see Zhou et al. 2003), careful case studies of CME events associated with filament eruptions are of great help in clarifying the relevant physics. So far, only a few prominence eruptions showing CME initiations have been observed from on-disk observations (e.g., Rust & Hildner 1976; Dere et al. 1997; Zhang & Wang 2000). Here we present a clear example in which the initiation process of the CME is well mapped by EUV Imaging Telescope (EIT) 304 and 195 Å observations. Unlike the previous cases, this eruptive prominence evolved quite slowly, which allows us to study each phase of the eruption in unprecedented detail, including its twisting, writhing, internal mass motion and/or mass draining, and final disruption. This example enables us to examine whether or not we can view the signature of a flux rope in a prominence eruption, what triggers the CME initiation, and at what stage the reconnection becomes important in a CME process. In § 2 we present a detailed description of the observations, and then we discuss what we can learn from the observations about CME physics in § 3.

2. OBSERVATIONS AND RESULTS

The eruption process of this event was observed by EIT at 304 and 195 Å with a cadence of 6 hr and 12 minutes, respectively.

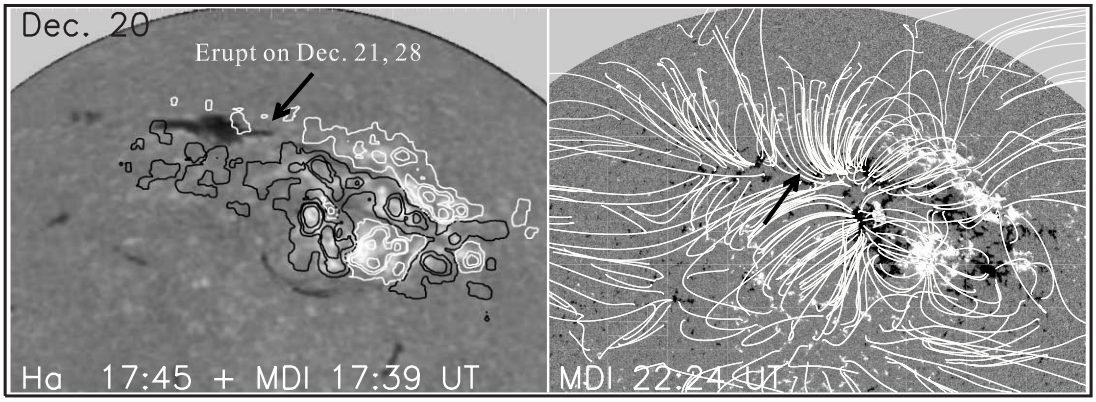

FIG. 1.—*Left panel:* Hα image on Dec. 20 is overlaid by a MDI data contour of the extended bipole region, the MDI data is smoothed by 10 pixels; the contour level is ±[10, 60, 100, 200, 500]; the arrow denotes an almost identical piece of the filament that erupted on December 21 and 28, both of which are associated with fast CMEs. *Right panel:* Reconstructed magnetic field lines by nonlinear extrapolations to show the multiple magnetic arcades over the filament. [*See the electronic edition of the Journal for a color version of this figure*.]

The Large Angle and Spectrometric Coronagraph (LASCO) observations are used to view the associated CMEs. Both EIT and LASCO are on board the *Solar and Heliospheric Observatory* (*SOHO*). In addition, the observations from the *Geostationary Operational Environmental Satellite* (*GOES*) soft X-ray (SXR) and *RHESSI* hard X-ray (HXR) are also used to study the high-energy process of this event.

The left panel of Figure 1 displays a long filament on 2002 December 20 in an Hα image from High Altitude Observatory. The filament was crossing the visible longitudes in the high latitudes of northern solar hemisphere. A near-time MDI magnetogram is contoured on the Hα image showing the filament in an extended bipolar region (EBR; see Zhou et al. 2005). Following the method of linear force-free extrapolations (Wang et al. 2001),

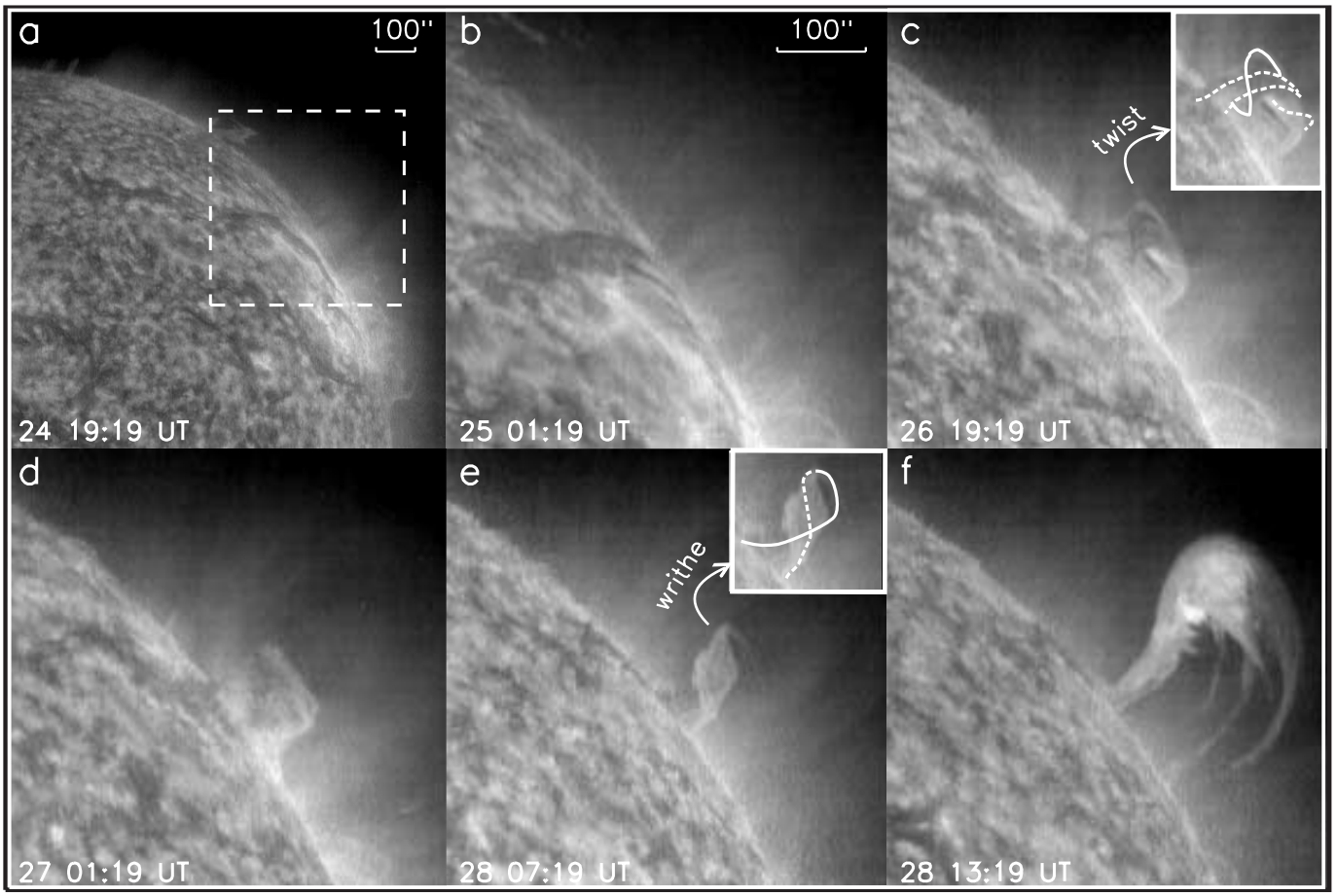

FIG. 2.—EIT 304 Å images show the prominence with the signature of the kink instability: (*b*–*d*) twisting, (*e*) writhing, and (*f*) erupting; the rectangle in (*a*) shows the field view of the other panels; the solid and dashed lines in the inset of (*c*) are used to trace the twists of the prominence fibers, one of which twists at least one turn (see the solid line) by apparent vision; the solid and dashed lines in the inset of (*e*) indicate the front and back legs of the writhed prominence; the panel scales are denoted in (*a*) and (*b*). [*This figure is available as an mpeg file in the electronic edition of the Journal.*]

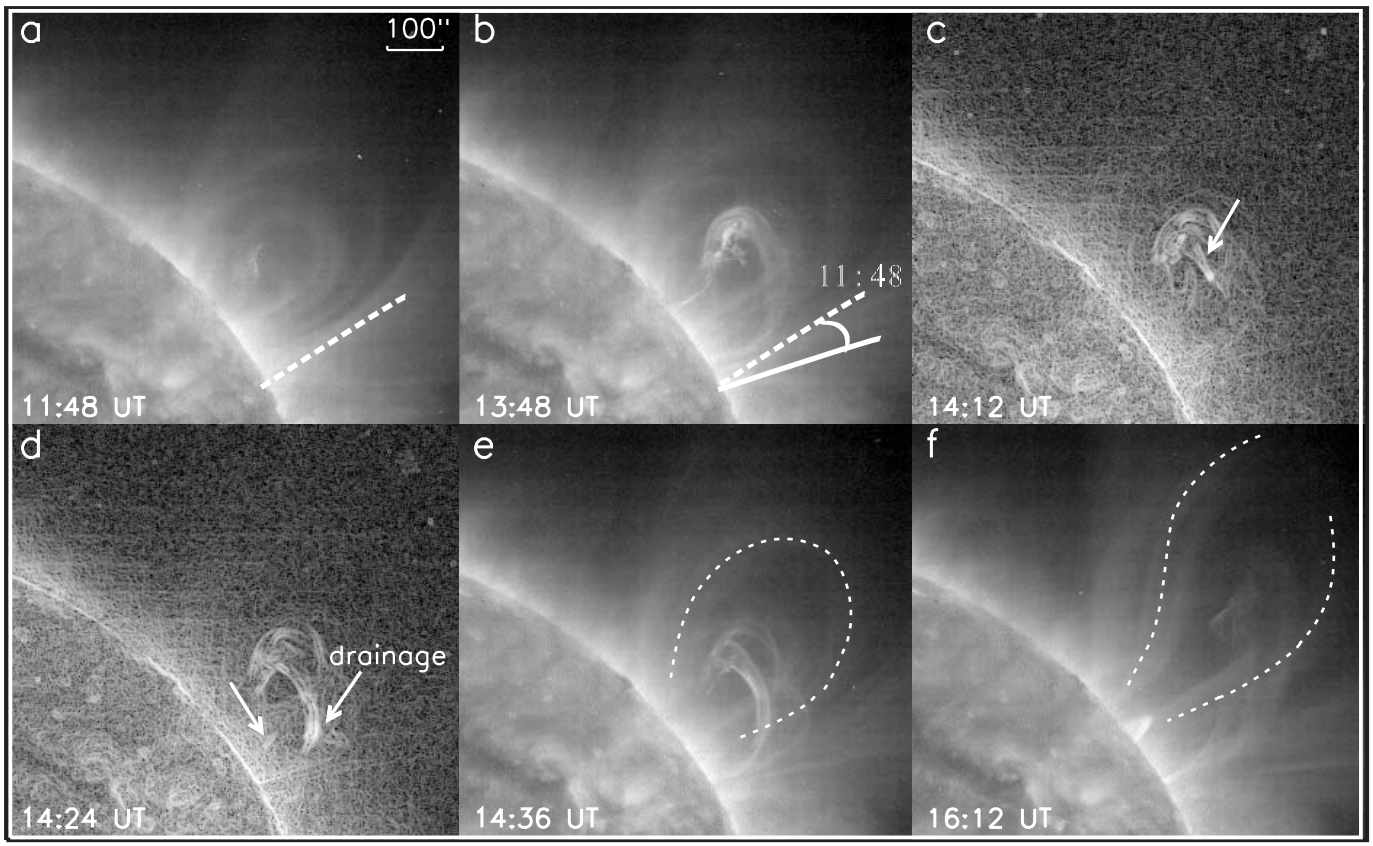

FIG. 3.—EIT 195 Å images show the prominence disruption with the combination of kink and drainage instabilities. Two lines forming an angle of significant magnitude in (*b*) indicate the same leg of the arcade envelope at 11:48 UT (*dashed*) and 13:48 UT (*solid*), respectively. The arrows in (*c*) and (*d*) denote the motion of material along the prominence legs. In order to show the mass drainage more clearly, in (*c*) and (*d*) the edges of the images are enhanced. Two dashed curves in (*e*) and (*f*) denote the outlines of the adjacent arcades. A cusp shape structure (*f*) appears after the prominence disruption; the length scale is shown in (*a*). [*See the electronic edition of the Journal for a color version of this figure*.]

the magnetic field lines are reconstructed based on the MDI data at 22:24 UT on December 20 (see Fig. 1, *right panel*). The extrapolation result indicates that there are multiple arcades overlaying the long filament. During its disk passage from 2002 December 20 to December 28, a part of the filament (see Fig. 1, *arrow in left panel*) was frequently disturbed and erupted, and triggered several CMEs. In this work we discuss the dynamics of the filament and the associated CME on December 28, when the filament appeared as a prominence above the northwest limb.

Figure 2 shows the EIT observations of the prominence eruption at the wavelength of 304 Å, in which the kink development of the prominence was clearly revealed (see also the EIT 304 Å animation in the online material). On early December 25, threads of the twisted prominence start to move upward (Figs. 2*b*–2*d*). We treat the twisting fibers as the signature of the prominence twists. The extent of the prominence twist is estimated not less than one turn, since one of the prominence fibers, as highlighted by a white solid line in the rectangle inset of Figure 2*c*, twists at least one turn by apparent vision. From 19:19 UT on December 26, the prominence is seen to be probably partially untwisting, and a fraction of the twist is converted to the writhe as required by the helicity conservation (Berger 1999). Unfortunately, during this interval, the signal of the prominence was so weak even in the high cadence EIT 195 Å images that the detailed evolution of the prominence from twist to writhe and partial eruptions could not be grasped. However, how the writhe of the prominence can be identified in an EIT 304 Å image of Figure 2*e*. The writhing prominence is traced by the white solid and dashed lines in the inset of Figure 2*e* to indicate its front and back legs. The prominence kept writhing until 11:48 UT on December 28, then it began to disrupt. Afterward, the prominence activation and eruption could be traced nicely by the high cadence EIT 195 Å images.

Figure 3 presents the EIT 195 Å images with higher cadence. At about 11:48 UT on December 28, the apex of the prominence began to brighten (Fig. 3*a*), and it became unstable, continuously ascending, unwrithing, and expanding (see Figs. 3*b*–3*d*). Its writhe is disentangled at about 12:24 UT. During the time interval of 11:48–13:48 UT, the prominence rose from 1.18 to about 1.30 $R_{\odot}$. Correspondingly, a propagating arc is seen by LASCO. In the following interval of 13:48 and 14:36 UT, the prominence became reactivated, showing ejecta with internal twisting and evidence of internal mass motions, hovering at a certain height but with an expanding profile before a catastrophe (Zhang et al. 2005). During this reactivation phase, some bright materials moved downward along legs of the prominence as indicated by the arrows in Figure 3*c* and 3*d*. After this activation phase, the prominence started a catastrophic eruption, moving outward drastically until ~17:00 UT, when it was out of the EIT field of view. Correspondingly, a CME is observed in the LASCO field of view. By checking *GOES* SXR and *RHESSI* HXR data, we find that the locations of all the 11 microflares during the period of 11:00–17:00 UT are from the southern hemisphere, this might exclude the possibility that the early stage of the prominence eruption is caused by magnetic reconnection. Later on, a cusp-shaped structure and postflare loops were observed, which becomes obvious at 16:12 UT (Fig. 3*f*) and at 20:12 UT, respectively.

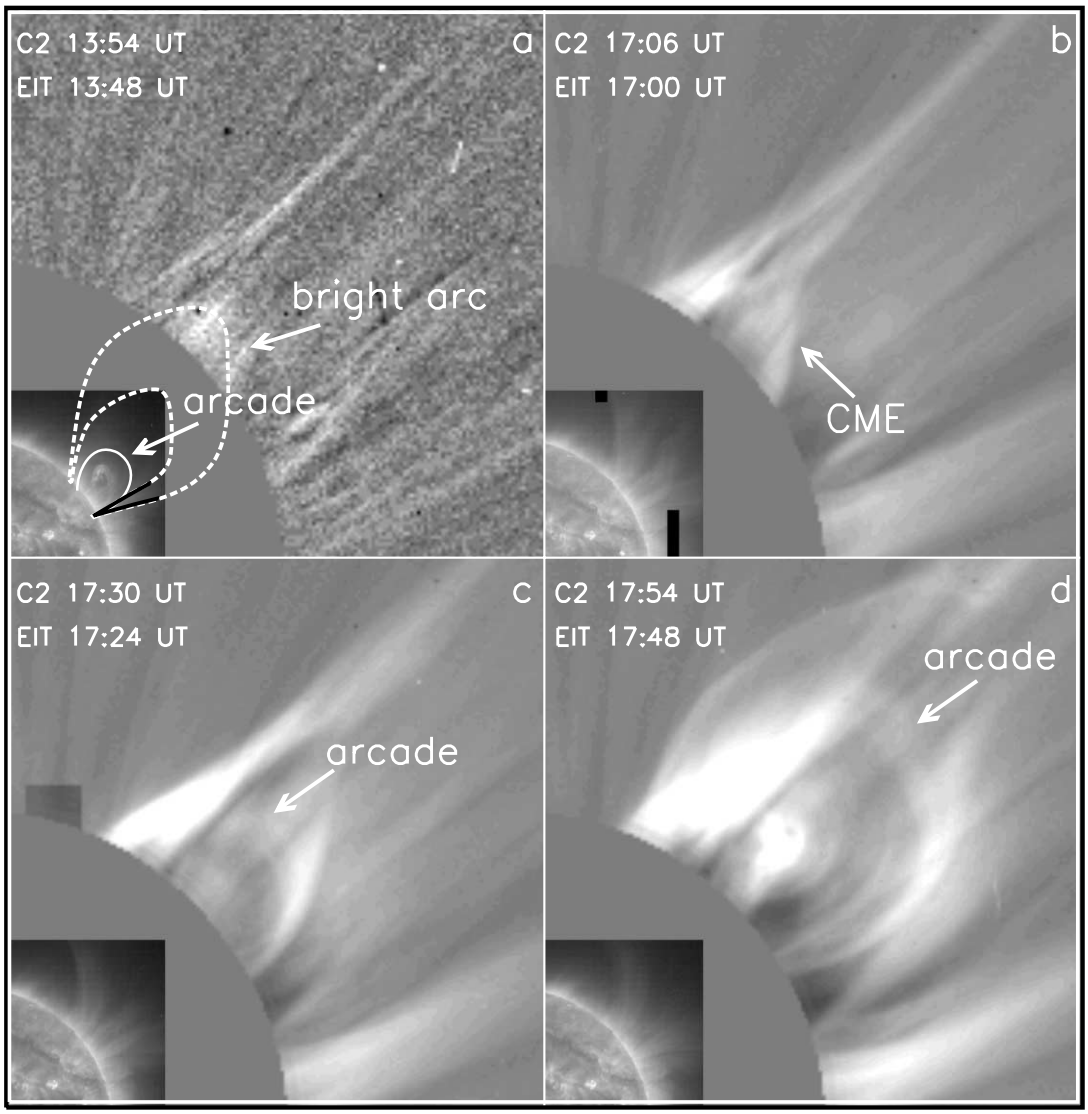

FIG. 4.—(*a*) LASCO/C2 running and (*b–d*) base difference images combining with EIT 195 Å images show the propagating bright arc (the arrow labeled "bright arc") and the CME with a core (arrow labeled "CME") associated with the prominence eruption. For each C2 base difference image we have subtracted a reference image at 12:54 UT. In (*a*) two dashed curves represent the whole envelope of the arcades whose one-leg orientations at two different times (*two solid lines forming an angle*) are also indicated in Fig. 3*b*. The dashed curves are manually traced out according to the observable orientations of the arcade envelope. The solid curve in (*a*) highlights the adjacent overlaying arcade that forms the CME front (see arrow labeled "arcade" in Figs. 4*a*, 4*c*, and 4*d*).

During the process of the prominence eruption, the multiple-layer overlaying arcades are driven to move upward and expand, as shown in Figure 3. The lines in Figures 3*a* and 3*b* denote the leg orientations of the EUV arcade envelope at times of 11:48 UT (*dashed line*) and 13:48 UT (*solid line*), respectively. Representing different orientations of the arcade leg, they are inclined with a significant angle, indicating an expansion of the arcade envelope. According to the orientations, we can approximately trace out the whole outer profile of the arcade envelope, which is presented as two dashed curves in Figure 4*a*.

Figure 4 shows the propagating bright arc and the CME. According to CME catalog,[1] both of them are recorded as CMEs with the projected speeds of about 399 and 901 km s^{-1}, respectively. As we have identified, at 13:54 UT, a little lump of bright coronal emission first appeared in LASCO/C2 field of view (see arrow labeled "bright arc" in Fig. 4*a*). Comparing EIT observations with LASCO/C2 images, we note that, at 13:54 UT, the arcade envelope also reached to this height by tracing the envelope (see Fig. 4*a*, *dashed curves*). Thus we tentatively suggest that the propagating bright arc corresponds to the successive rearrangement of the closed field lines overlying the filament, as explained in Chen et al. (2002).

At 16:30 UT, another lump with much brighter coronal emission was observed (see arrow labeled "CME" in Fig. 4*b*), then the front became brighter and brighter and was followed by a bright core, as seen from C2 images at 17:54 UT (Figs. 4*c*–4*d*). From the above analysis, we suggest that the initiations of the propagating bright arc and the CME were the results of the continuous disturbance and eruption of the prominence, respectively.

Assuming that the CME leading edge originates from the UV arcade overlying the prominence and that the CME core corresponds to the ejected prominence material, we can follow the erupted prominence and its adjacent overlaying arcade from EIT 195 Å images (see the curves in Figs. 3*e* and 3*f*, and the dashed curves in Fig. 4*a*) to C2 images by measuring their heights. The time evolution of the logarithmic heights for both the filament

[1] See http://cdaw.gsfc.nasa.gov/CME_list.

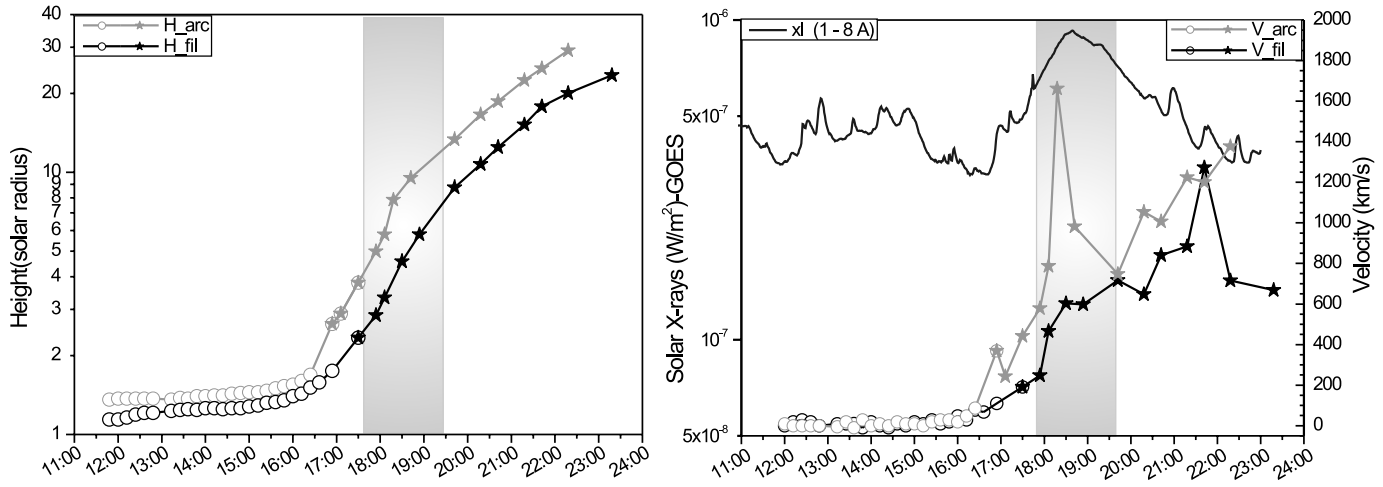

FIG. 5.—Time profile of logarithmic height (*left*) and velocity (*right*) for the eruptive prominence (*bottom curve*) and its adjacent overlaying arcade (*top curve*). For comparison, the curve without symbols observed by *GOES* is overlaid On the right. The shaded areas indicate the reconnection phase after the prominence eruption. In the lines with different symbolsm of circles and asterisks indicate the data from the field of view of EIT and LASCO, respectively. [*See the electronic edition of the Journal for a color version of this figure.*]

and the arcade are given in the left panel of Figure 5, while the derived velocity curves are shown in the right panel of Figure 5. The height-time plots present two smooth curves, indicating that the above assumptions are valid. It is worth noting that both velocity curves have an obvious increase, especially for the arcade velocity, which is in coincidence with a gradual rise of the *GOES* 1–8 Å soft X-ray flux. However, no corresponding flare was reported by *GOES* observations.

The further information about the initial acceleration of the prominence eruption and the related magnetic reconnection can

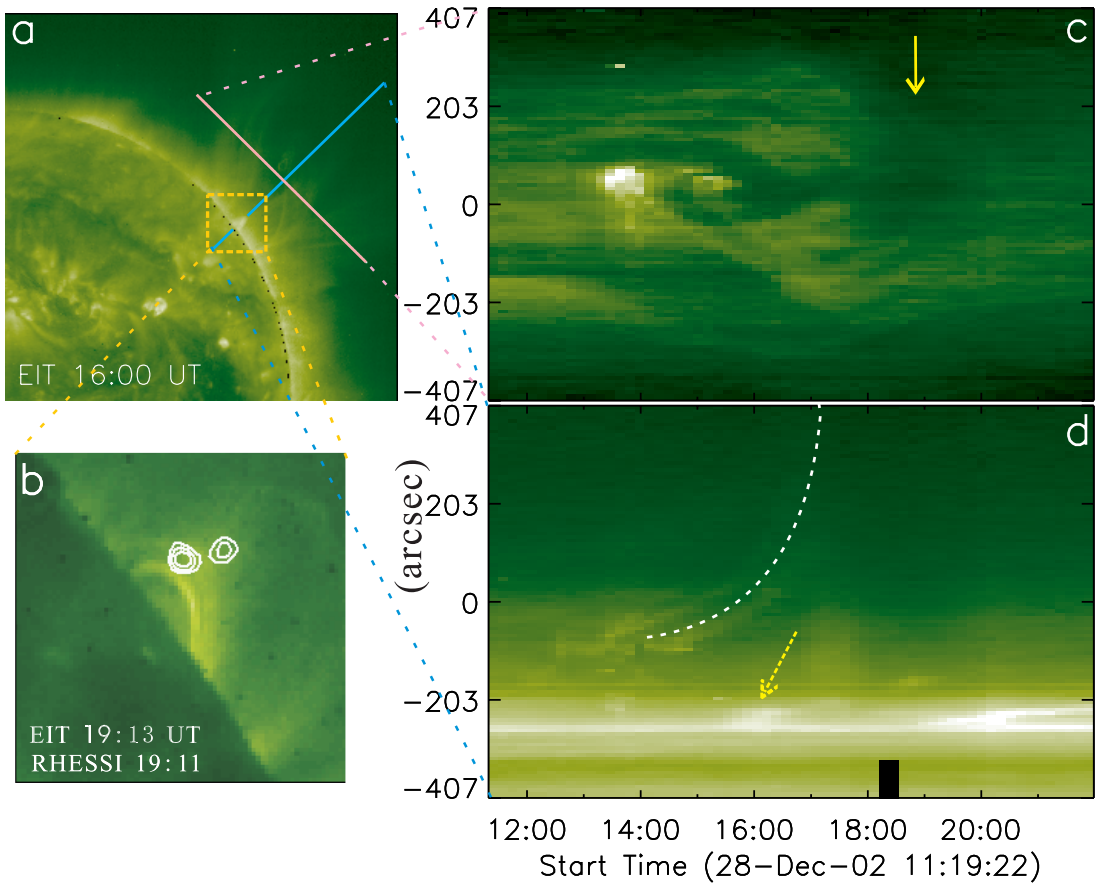

FIG. 6.—Time evolutions of EUV intensity in (*c*) and (*d*) are along the pink and blue lines (*a*) from 11:19 to 22:00 UT. The pink and the blue lines are perpendicular to and run across the bisector of the cusp structure (see *a*), respectively. In order to reveal the cusp structure, a small part of the blue line overlying the cusp structure has been removed. Panel *b* is the enlarged image of the quadrate part of (*a*). White contours in (*b*) denote the position of a X-ray emission in the energy range of 3–9 keV as observed by *RHESSI*.

TABLE 1
TIME SEQUENCES OF CME INITIATION

Date	Time (UT)	Phenomena
25.....	00:36	A part the long filament began to rise
25.....	01:19	The twist of the prominence was discernible
27.....	01:19	The prominence began to writhe
28.....	11:48	The apex of the prominence began to brighten in 195 Å images
	11:48–13:48	The prominence was slowly ascending, probably untwisting, and expanding continuously
	13:48–14:36	Reactivation phase of the prominence before its catastrophic eruption
	13:54	A propagating bright arc appeared in LASCO/C2 images
	14:36–15:24	The prominence disrupted cusp shape structure first appeared
	16:30	The associated CME appeared
	16:48	The apex part of the prominence ran out of the EIT field of view
	17:30	The core of the CME first appeared
	18:12	Postflare loop first appeared
	18:50–19:11	Weak HXR source appeared on the top of postflare loops

well be seen in Figure 6. Figure 6*b* is a *RHESSI* map (*contour lines*) at 19:11 UT overlaid on an EIT subimage (see Fig. 6*a*, *yellow dashed rectangle*) in the near time of 19:13 UT. The *RHESSI* map shows emissions below the erupting filament and arcades and on the top of the postflare loop after the filament eruption. It hints that magnetic reconnection will probably occur around the stretched magnetic field lines, which produces the cusp structure and loop-like emissions, as observed in the EIT 195 Å images. Figures 6*c* and 6*d* are time evolutions of the one-dimensional distribution of EUV intensity along two solid lines (Fig. 6*a*, *pink and blue solid lines*) from 11:24 to 22:00 UT. One of the two lines in Figure 6*a* is almost perpendicular to the cusp structure (*pink line*), and the other one centralizes in the bisector of the cusp structure (*blue line*). As indicated by the yellow arrow in Figure 6*c*, a converging structure appears after the bright prominence passed the line, which is strongly suggestive of the occurrence of magnetic reconnection (Yokoyama et al. 2001; Chen et al. 2004). In addition, in Figure 6*d* the eruptive prominence presents a parabola-like upward motion (*denoted by dashed curve*), which indicates a constant acceleration from 14:36 UT, long before the cusp structure formed when magnetic reconnection occurs (*see the yellow arrow*). So the prominence disruption at this stage is not driven by magnetic reconnection that is manifested by the cusp structure, postflare loops, and *RHESSI* hard X-ray sources. Magnetic reconnection may contribute to the further acceleration of the eruption of the filament and arcades in the later phase, as indicated by the right panel of Figure 5. The time sequence of the CME initiation is listed in Table 1.

3. CONCLUSIONS AND DISCUSSION

The observed scenario for this event can be schematically shown in Figure 7, which briefly illustrates its four evolving phases. (1) Before being disturbed, a part of the long filament became strongly twisted and was overlaid by multiple-layer arcades at different heights (Fig. 7*a*). The prominence twisted not less than one turn, which exceeds the critical value for the kink instability (Hood & Priset 1979). (2) As the kink instability developed, the prominence rose and converted part of its twist to writhe, so

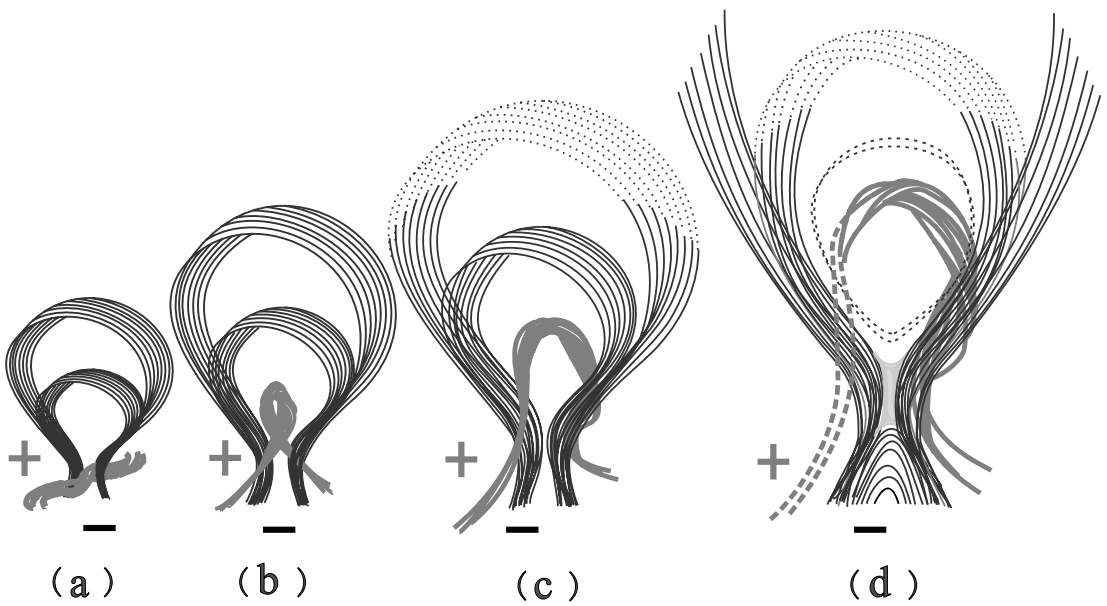

FIG. 7.—Cartoon demonstrating the scenario of the event. (*a*) Before the eruption, the prominence presents twist; (*b*) with a kink instability, the prominence converts part of its twists to writhes; (*c*) under the combinations of kink and drainage instabilities, the prominence rises and expands, impelling its arcades moving upward to form the propagating bright arc; and (*d*) the prominence reactivates and disrupted in the end, causing the CME with a core. Magnetic reconnection occurs in a current sheet (see the light colored area above the cusp structure in panel *d*) after the prominence disruption. Dashed lines incicate possible structures that cannot be observed clearly in EIT field of view. [*See the electronic edition of the Journal for a color version of this figure.*]

the prominence and its arcades reached a new height (Fig. 7*b*). (3) While the prominence was rising, some materials in the prominence might have drained back to the solar surface along the deformed field lines (Fig. 7*c*), producing the magnetic buoyancy force to impel the prominence to rise again. During this phase, the overlying arcades were driven to rearrange with gradual ascensions and expansions. They are observed as the propagating bright arc in the field view of LASCO/C2. (4) The prominence is reactivated, manifested by its internal twisting and mass motion for approximate 40 minutes. Then the prominence erupted and its adjacent arcade ascended and restructured to form the CME with a bright core. The reconnection at the current sheet (see the light colored area in Fig. 7*d*) in the wake of the erupted prominence led to an additional drastic acceleration of the prominence and its overlaying arcades for the CME.

By studying this example, several key issues related to the CME initiation can be addressed. First, the current example demonstrates that only a fragment of the very long filament erupted in this event, which led to a propagating bright arc and a CME. The long filament lies on the magnetic neutral line of an EBR. Looking back into the history of the filament activity, we found that, at almost the same location of the eruptive fragment in this event, a part of the filament erupted approximately at 23 : 12 UT on December 20, which led to a halo CME. The filament restored quickly after the CME. It is unlikely that the very long filament presented a single magnetic flux rope as suggested by Rust & Kumar (1994). It seems that not a presubmerged flux rope, but the general magnetic environment, e.g., the EBR, created the long filament and the episodic eruption of its fragments that then became the CME. The repeated eruptions at almost the same part of the filament are indicative that the local magnetic evolution underneath the filament is important too in triggering the eruption. From the observations, we have no direct evidence whether or not there is a flux rope, representative to the erupted prominence. Even if there was a flux rope, we should be honest and say that it was the large-scale magnetic configuration together with the localized magnetic evolution that created the flux rope. Unfortunately, the current observations provide no hints about flux rope creation and development.

Second, it is quite reasonable to state that the filament and its overlying arcades evolve to be the CME. In particular, the prominence arcades become the bright front of the CME, while the erupted prominence itself corresponds to the bright core of the CME. The prominence and its arcades seem to be a coherent system, they were accelerated synchronously during the CME process (see the left panel of Fig. 5*c*). However, in this event one has no way to diagnose physically what is the dark cavity of the CME. No physical entity in either the prominence system or the observed CME can be identified to be the dark cavity.

Third, the propagating bright arc and the early eruption of the CME are initiated primarily by the kink and buoyancy instabilities of the prominence as an ideal MHD process. Magnetic reconnection took place during the later rapid eruption of the CME, which was indicated by the formation of the cusp structure, the postflaring loops, and the hard X-ray source that are commonly regarded as the signatures of magnetic reconnection. The reconnection did impulsively accelerate the prominence and its arcades. It cannot be fully excluded that magnetic reconnection had taken place among individual prominence threads during the kink instability, or that there was magnetic reconnection in the lower solar atmosphere (e.g., flux cancellation) that made the filament twist and kink.

Finally, mass drainage seems to play an important role in triggering the eruptions. During the activation phase, some materials in the prominence are seen to drain to the solar surface. Assuming that the materials experience a free fall from the apex of the prominence to the solar surface along a quarter-circle, it will take about 42 minutes, which is close to the duration of the prominence reactivation phase. So we suggest that gravity may play an important role, through mass drainage, in triggering the onset of CMEs, as proposed by Low (2001).

The work is supported by the National Natural Science Foundation of China (G10573025, G10233050, 10403003, and G40504021) and the National Key Basic Research Science Foundation (2006CB8060300). *SOHO* is a project of international cooperation between ESA and NASA.

REFERENCES

Antiochos, S. K., Dahlburg, R. B., & Klimchuk, J. A. 1994, ApJ, 420, L41
Antiochos, S. K., DeVore, C. R., & Klimchuk, J. A. 1999, ApJ, 510, 485
Berger, M. 1999, in in Magnetic Helicity in Space and Laboratory Plasmas, ed. M. R. Brown, R. C. Canfield, & A. A. Pevtsov (Washington: AGU), 1
Bety, H. 2001, A&A, 367, 321
Chen, P. F., & Shibata, K. 2000, ApJ, 545, 524
Chen, P. F., Shibata, K., Brooks, D. H., & Isobe, H. 2004, ApJ, 602, L61
Chen, P. F., Wu, S. T., Shibata, K., & Fang, C. 2002, ApJ, 572, L99
Dere, K. P., et al. 1997, Sol. Phys., 175, 601
Fan, Y., & Gibson, S. E. 2004, ApJ, 609, 1123
Feynman, J., & Martin, S. F. 1995, J. Geophys. Res., 100, 3355
Forbes, T. G., Priest, E. R., & Isenberg, P. A. 1994, Sol. Phys., 150, 245
Gerrard, C. L., Arber, T. D., Hood, A. W., & Van der Linden, R. A. M. 2001, A&A, 373, 1089
Gilbert, H., Holzer, T. E., Burkepile, J. T., & Hundhausen, A. J. 2000, ApJ, 537, 503
Gosling, J. T. 1993, J. Geophys. Res., 98, 18937
Hood, A. W., & Priset, E. R. 1979, Sol. Phys., 64, 303
Hu, Y. Q. 2005, in Proc. IAU Symp. 226, ed. K. Dere, J. X. Wang, & Y. Y. Yang (Cambridge: Cambridge Univ. Press), 263
Lin, J., & Forbes, T. G. 2000, J. Geophys. Res., 105, 2375
Low, B. C. 2001, J. Geophys. Res., 106, 25141
Mikic, Z., & Linker, J. A. 1994, ApJ, 430, 898
Plunkett, S. P., et al. 2000, Sol. Phys., 194, 371
Rust, D. M. 2003, Adv. Space Res., 32, 1895
Rust, D. M., & Hildner, E. 1976, Sol. Phys., 48, 381
Rust, D. M., & Kumar, A. 1994, Sol. Phys., 155, 69
Rust, D. M., & LaBonte, B. J. 2005, ApJ, 622, L69
Sakurai, T. 1976, PASJ, 28, 177
Tandberg-Hanssen, E. 1974, Solar Prominences (Dordrecht: Reidel)
Török, T., & Kliem, B. 2005, ApJ, 630, L97
Wang, H., Yan, Y., & Sakurai, T. 2001, Sol. Phys. 201, 323
Williams, D. R., Török, T., Démoulin, P., van Driel-Gesztelyl, & Kliem, R. 2005, ApJ, 628, L163
Yokoyama, T., Akita, K., Morimoto, T., Inoue, K., & Newmark, J. 2001, ApJ, 546, L69
Zhang, J., et al. 2001, ApJ, 548, L99
Zhang, J., & Wang, J. X. 2000, Geophys. Res. Lett., 27, 2877
Zhang, Y. Z., Hu, Y. Q., & Wang, J. X. 2005, ApJ, 626, 1096
Zhang Y. Z., Wang, J. X., & Hu, Y. Q. 2006, ApJ, 641, 572
Zhou, G. P., Wang, J. X., & Cao, Z. L. 2003, A&A, 397, 1057
Zhou, G. P., Wang, J., & Zhang, J. 2006, A&A, 445, 1133